Assessment of Sound Radiation of semi-buried Engine Intakes

Thomas Lauke, Markus Lummer, Roland Wilhelm
DLR Institute of Aerodynamics and Flow Technology
P. O. Box 32 67
38022 Braunschweig
Germany

Abstract

The sound radiation from the intake of unconventional aeroengine intakes was studied computationally. The configuration is characterized as a nacelle which is buried into an aerodynamic surface (fuselage or wing) with various burying levels. The influence of the flow field on the sound radiation was studied as well.
After generating a curvilinear structured 3D multi-block grid for the given configuration, the precalculated solution of DLR's CFD finite volume code Tau was interpolated from its unstructured mesh onto the structured one for the acoustic calculations. The simulation of aeroacoustic propagation out of the engine inlet was performed using DLR's CAA code PIANO (**p**erturbation **i**nvestigation of **a**erodynamic **no**ise), which solves the (non)linear Euler perturbation equation. PIANO is a high resolution, high order finite difference code advancing the numerical solution in time by the well known 4-stage Runge-Kutta scheme. Spatial derivatives are discretized by the **d**ispersion **r**elation **p**reserving (DRP) scheme of C.K.W. Tam et. al. A 4^{th}-order pade filtering is used to eliminate spurious waves. As a generic source plane waves of 1000 Hz (blade passing frequency) were enforced by a sponge-layer technique to enter the duct from downstream of the given fan face position (i.e. in the unphysical duct extension). For two levels of burying the case without flow served as a reference. The spatial structure of the sound field was evaluated on distinct sections (symmetry, i.e. $y = 0$, and ground plane, i.e. $z = 0$) of the three-dimensional computational domain. The directivities in the planes of three circles (perpendicular to each other) were determined by recording the pressure time histories.
The influence of different mean flows as well as burying levels was proven. Contrary to the $^1/_2$-buried case the $^1/_3$-buried geometry causes a non-axi-symmetric lateral directivity without flow. It could be demonstrated how an only locally too poor grid resolution may result in a completely non-physical solution. The actual viscous mean flow plays an important role, especially because of its (even poorly resolved) boundary layers. The results underline the need of using a perturbation approach of LEE type to describe the physics of the sound radiation from a buried intake properly. No self sustained flow oscillations (resonances) were observed in any considered case.

Introduction

The studies performed on future concepts of aircraft of very high passenger capacity have identified potential benefits in terms of fuel burn reduction with innovative concepts, such as the flying wing or the wide fuselage aircraft. These new aircraft would undoubtedly lead to non typical engine installations, such as the buried or the rear-fuselage installations. In the same time, the constraints related to environmental issues could become more and more drastic in the future, and the developments of new aircraft concepts could be driven by parameters other than just economics or range and speed performance. The competitiveness of aircraft could be increasingly influenced by environmental factors, such as the noise emissions.

The 18 month lasting Airbus-EREA project SeBu (**Se**mi-**bu**ried Engine for Advanced Aircraft Concepts) was devoted to the investigations of the specific issues raised by such engine installation configurations, in the domains of aerodynamics, noise emissions, structural behaviour and vibration

propagation. During this project the following method for the early design phase of aircraft was developed in order to assess the sound radiation characteristics of semi-buried engine intakes.
The paper is structured into three sections: First the problem is presented; the configurations investigated are defined along with the operating conditions. Section 2 is devoted to the aerodynamic investigations, while the third section is dealing with the aeroacoustic aspects of the sound radiation out of the intake.

1. Definition of configuration and operating conditions

The configuration considered is a local component of the aircraft, representing the rear part of the fuselage of a new concept of aircraft of flying wing type, with the engine installed on the upper side of the fuselage and partly integrated inside it. The powerplant installation is composed of the inlet, a S duct, the engine and a nozzle. The shapes and configurations considered are generic ones, with the objective of identifying the phenomena and prediction schemes, more than designing a shape with optimised performances. The configurations are composed of an axi-symmetric inlet shape intersected by a flat plate, representing a part of the fuselage (Figure 1). Two configurations are considered, corresponding to two levels of burying the engine inside the fuselage: one-half and one-third of the inlet throat diameter.

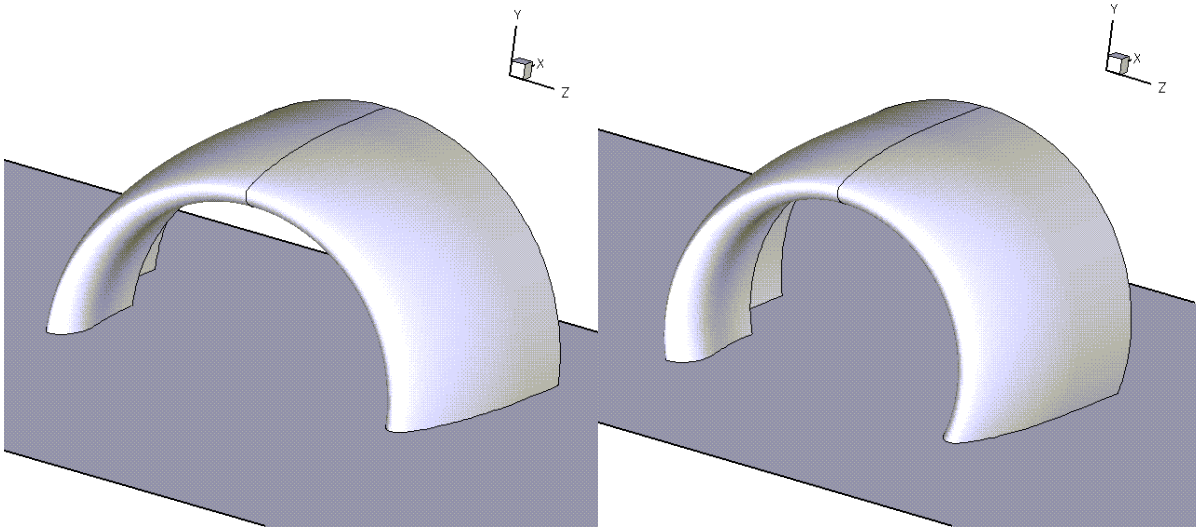

Figure 1: Schematic views of the semi-buried inlets – $^1/_2$-buried (left) and $^1/_3$-buried (right)

The general dimensions of the inlet were defined by Airbus France:

- Inlet length equal to 1.70 m;
- Fan area equal to 6.80 m^2 (diameter 2.95 m);
- Throat area between 6.10 m^2 and 6.20 m^2 (A_{fan}/A_{throat} around 1.10);
- Highlight area around 7.7 m^2 ($A_{highlight}/A_{throat}$ about 1.25).

In order to have a meaningful comparison between the two configurations, it was necessary that all intake area ratios ($A_{highlight}/A_c$, $A_{highlight}/A_{fan}$, A_{fan}/A_{throat}) remained identical. This resulted in two different axi-symmetric profiles for the two inlets. The flow parameters are listed in the following table:

Mach	Static pressure [Pa]	Static temperature [K]	Reynolds per meter
0.25	101320.	288.	$5.85\ 10^6$

The operating conditions are the following ones:

Free stream velocity [m/s]	Corrected massflow [kg/s]	Massflow [kg/s]	Massflow ratio Epsilon (= A_∞/A_{fan})	Average Mach number in fan plane	Average static pressure in fan plane
85.0	1270.	1318.	1.860	0.527	87590.

The radiation of sound waves with the blade passing frequency of $f = 1$ kHz was to be investigated. This corresponds to a dimensionless wavenumber $kR = 27.3$; $k = 2\pi f/a$ being the wavenumber with the speed of sound a.

2. Aerodynamics of the air inlet

Computations

Unstructured finite-volume grids were generated with the grid generation package Centaur. In order to obtain a good resolution of the viscous boundary layer, 32 prismatic control volumes were generated near the walls to cover the complete viscous boundary layer. The remaining computational domain is discretized using pyramidal and tetrahedral control volumes (see Figure 2). During the calculations, the grids were adapted three times with respect to y^+ (targeted first grid point height y^+ around 1.0) and to the flow field solution. Finally the grid consisted of about 2.13 million nodes. The computational domain starts 40 m in front of the intake and extends 30 m to the side and aft of the configuration. The intake is 1.7 m long and cylindrically extended for computational purpose.

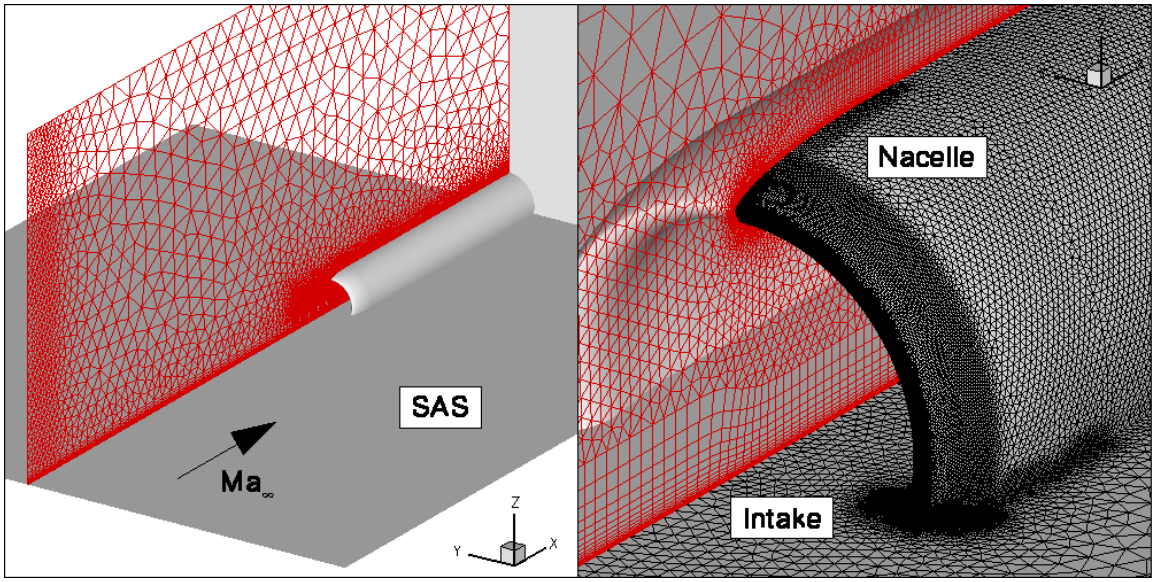

Figure 2: Computational domain (left, walls shaded) and triangular surface grid (right) for the 1/3-buried configuration

The flow solver used is the DLR Tau code, a finite-volume flow solver for the solution of the Reynolds-averaged Navier-Stokes equations on arbitrary grids. The code uses central differences and a 2nd order dissipation scheme for the discretization in space. The time integration is done with a 3-stage Runge-Kutta time-stepping scheme. For the calculations at low speed, preconditioning is enabled too. The one-equation turbulence model of Spalart-Allmaras with the modification of Edwards and Chandra and the two-equation Menter SST turbulence model were used for the calculations. The engine intake boundary used a constant pressure boundary condition which automatically establishes the desired engine massflow via static pressure adjustment. An inflow boundary

condition was used to prescribe a user-specified inflow velocity profile on the flat plate at the inflow of the computational domain.

Results

A burying level influence is shown in Figure 3 at Mach number 0.25 and for a boundary layer height of 0.6 m. The iso-Mach contours in the symmetry plane show that the flow field accelerates in the intake but does not reach supersonic velocities at the throat. No flow separation occurs in the intake. The surface pressure coefficients show that the same minimum pressure level is reached for the two configurations in all circumferential cuts, except at 108° for the $^1/_3$-buried configuration. The pressure values close to the leading edge are similar for the $^1/_2$-buried configuration in all circumferential cuts, whereas the pressures are higher close to the flat plate for the $^1/_3$-buried inlet: the merger region between the flat plate and the intake contour for the $^1/_3$-buried configuration decelerates the flow field around the leading edge.

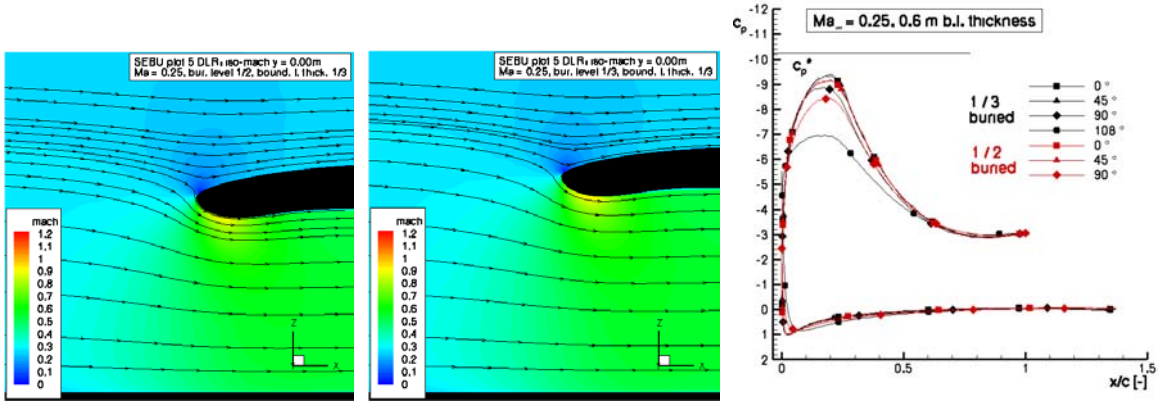

Figure 3: Burying level influence at Mach 0.25 - Iso-Mach contours in symmetry plane for $^1/_2$-buried (left) and $^1/_3$-buried (middle) inlets – c_p distributions (right)

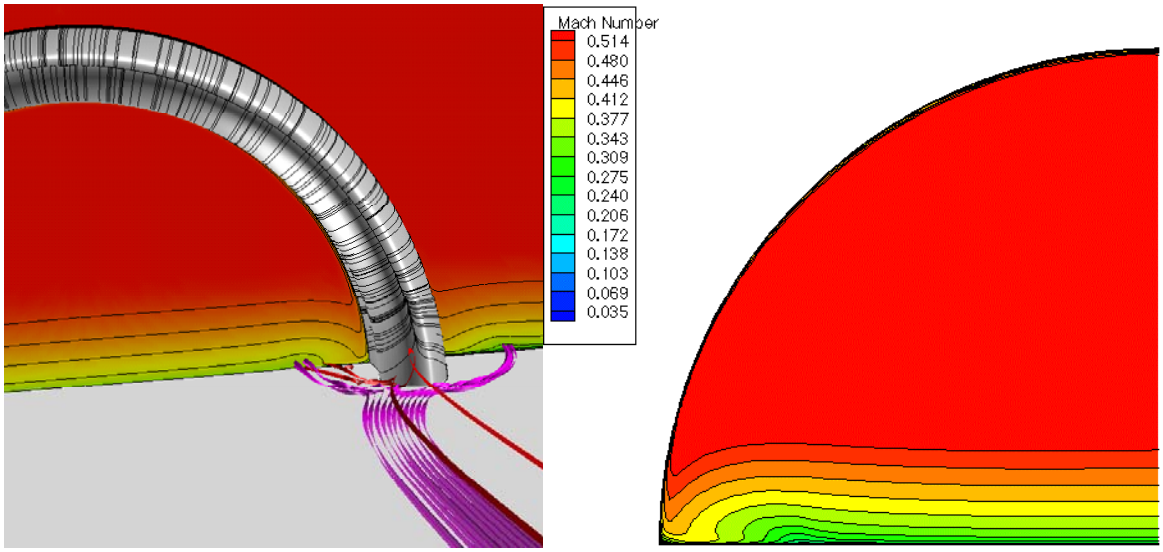

Figure 4: Intake spillage (left) and Mach number contours in throat plane (right), $^1/_2$-buried intake

The mechanism responsible for this is the tendency of the flow to roll-up in the form of a horseshoe vortex around the cowl/fuselage intersection (Figure 4, left part). This can be seen in the throat plane Mach number contours, when plotted on a suitable scale (Figure 4, right part).

3. Aeroacoustic investigations

DLR's CAA-Code PIANO simulated the acoustic field of fan tones being radiated out of the inlet to the free field, originating from within the housing of the intake.

Numerical Method

The DLR MegaCADs grid generator (**m**ulti-block **e**lliptic **g**rid generation **a**nd **CAD** **s**ystem) was used to generate a curvilinear multi-block structured mesh of 11 blocks (up to 4.2 million nodes) based on a parametric (burying level) script. To avoid a line singularity, a rectangular block was introduced on the symmetry axis as shown in Figure 5. The topology of the grids for both configurations ($^1/_2$- and $^1/_3$-buried) is identical; only minor differences occur due to geometric modifications (different nodes number in intake height e.g.). The computational domain starts 10 m in front of the intake and extends 10 m to the side and 6 m to the rear end. Dashed lines in the left part show three circles, perpendicular to each other, on which the data for directivity postprocessing is recorded. The right part illustrates the basic two-dimensional grid, which is rotated around the fan axis to obtain a three-dimensional mesh.

The in-house interpolation tool INTERPOL was used to linearly interpolate the unstructured CFD flow field data produced with the CFD code Tau onto the structured grid for the CAA-perturbation simulation.

The 3D-CAA code PIANO (**p**erturbation **i**nvestigation of **a**erodynamic **no**ise), solving the (non)linear Euler perturbation equation, performed the simulation of aeroacoustic propagation out of the engine inlet. PIANO is a high resolution, high order finite difference code advancing the numerical solution in time by the well known 4-stage Runge-Kutta scheme. Spatial derivatives are discretized by the dispersion relation preserving (DRP) scheme of C.K.W. Tam et. al. A 4th-order pade filtering is used to eliminate spurious waves. As a generic source plane waves of 1000 Hz (blade passing frequency) and amplitude $A = 1$ were enforced to enter the duct from downstream of the given fan face position (i.e. in the unphysical duct extension) by a sponge-layer technique. For both analysed configurations, computations without flow were done as a reference. For the assessment of geometry effects the pressure time histories on three circles (perpendicular to each other) were recorded. The spatial structure of the sound field was evaluated on distinct sections (symmetry, i.e. $y = 0$, and ground plane, i.e. $z = 0$) of the three-dimensional computational domain. The directivities in the planes of the aforementioned circles were determined.

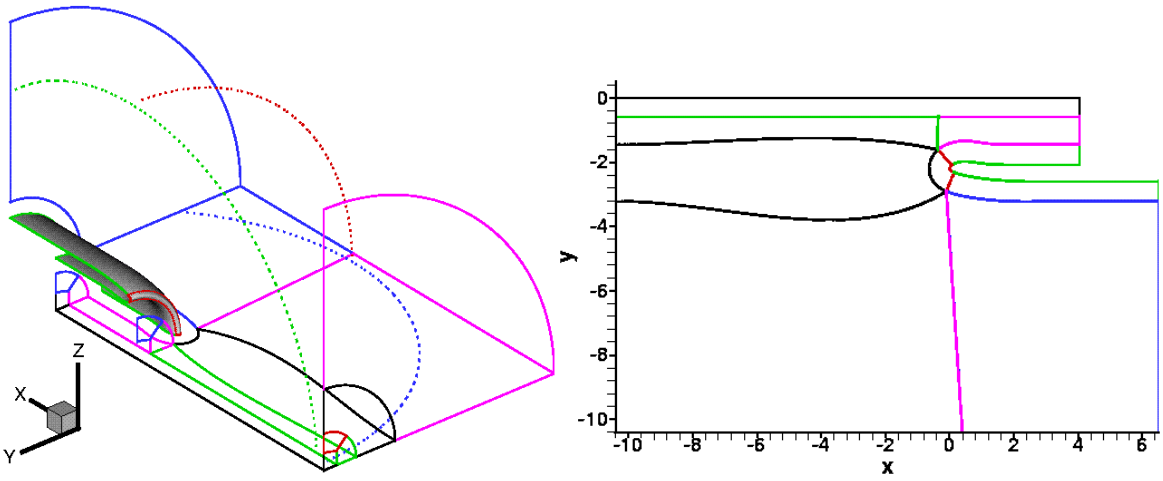

Figure 5: Topology for 11 blocks structured grid (left), basic 2D grid (right)

Analysis of acoustic results

Comparison of mesh refinement

Figure 6 demonstrates the importance of local mesh refinement in the throat area of the engine: less than 3 % additional nodes in the region with accelerated flow turns an unphysical solution (Figure 6 left) to a physical one (Figure 6 right). On the left clearly an unphysical radiation pattern is seen, while the right part of the figure shows the expected multilobed typical radiation pattern for the $^1/_2$-buried inlet at 1000 Hz, for a freestream flow at Mach number 0.25. The problem occurs when the sound waves are underresolved near the engine throat. Here the waves undergo a considerable reduction in wavelength due to local Mach numbers larger than 0.8. Figure 7 gives a detailed view of the refined region, mesh and solution as well.

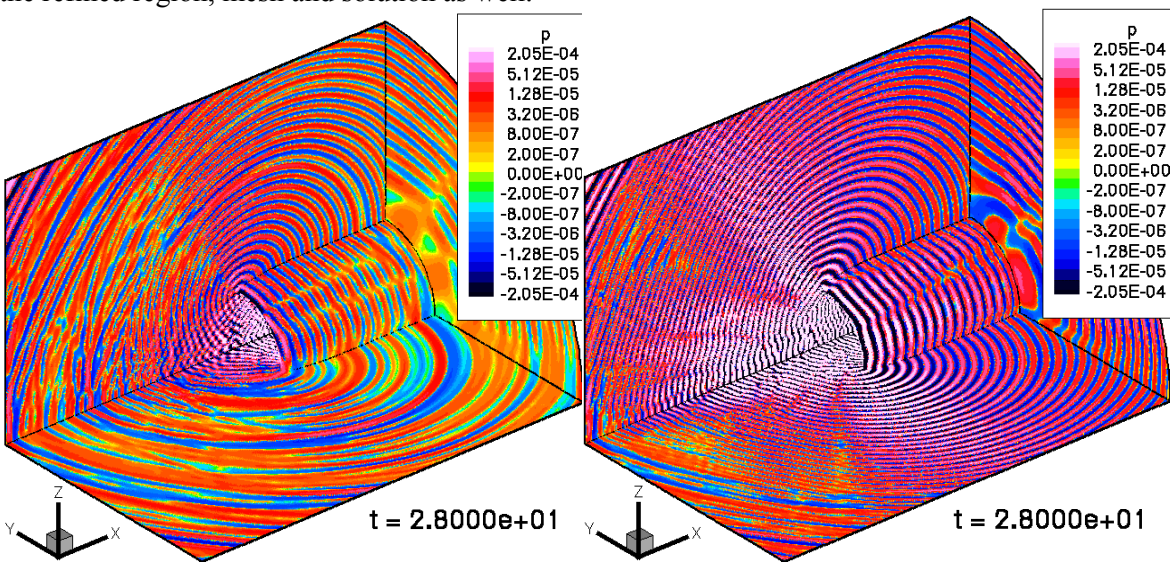

Figure 6: Influence of grid refinement with flow at Mach 0.25 and frequency 1000 Hz: original mesh (left), suitably refined mesh (right) for $^1/_2$-buried inlet; total view

Qualitatively the radiation phenomena for 500 Hz and 1000 Hz turned out to be similar, except a different pressure level and lobe-structure, as shown in Figure 8. For the sake of reduced computational costs it was therefore justified to reduce the frequency to 500 Hz for most simulations and study the flow effects on the radiation for this frequency.

Comparison of different mean flows

In Figure 9 is shown the influence of the flow field on the propagation phenomena. On the left side may be recognised the axi-symmetric radiation pattern without flow, the highest intensity of radiation is found in the upstream direction. On the right side, with the mean flow at Mach number 0.25 and a suction due to the engine massflow, a considerable modification of the directivity is observed. The same influence can be observed in Figure 10 for the $^1/_3$-buried inlet: in this case already without flow a non-axi-symmetric solution is obtained. This is shown again in the left part of Figure 15 in which a multilobed directivity is seen instead of a simple quarter circle distribution.
A quite beneficial radiation phenomenon is observed due to the presence of the boundary layer on the ground plane. Figure 13 shows that the intensity of the pressure signals appears to be reduced in the ground plane compared to the symmetry plane. Noise is strongly refracted out of the ground plane due to the presence of the ground plane boundary layer. This refraction effect accumulates with the distance along which the sound waves travel against the sheared flow near the ground plane. The directivity in the symmetry plane (right top of Figure 15) underlines the formation of a kind of zone of silence. This effect may have important consequences for semi-buried intake configurations since the refracted noise cannot be further diffracted down at any upstream edges of the actual aircraft.

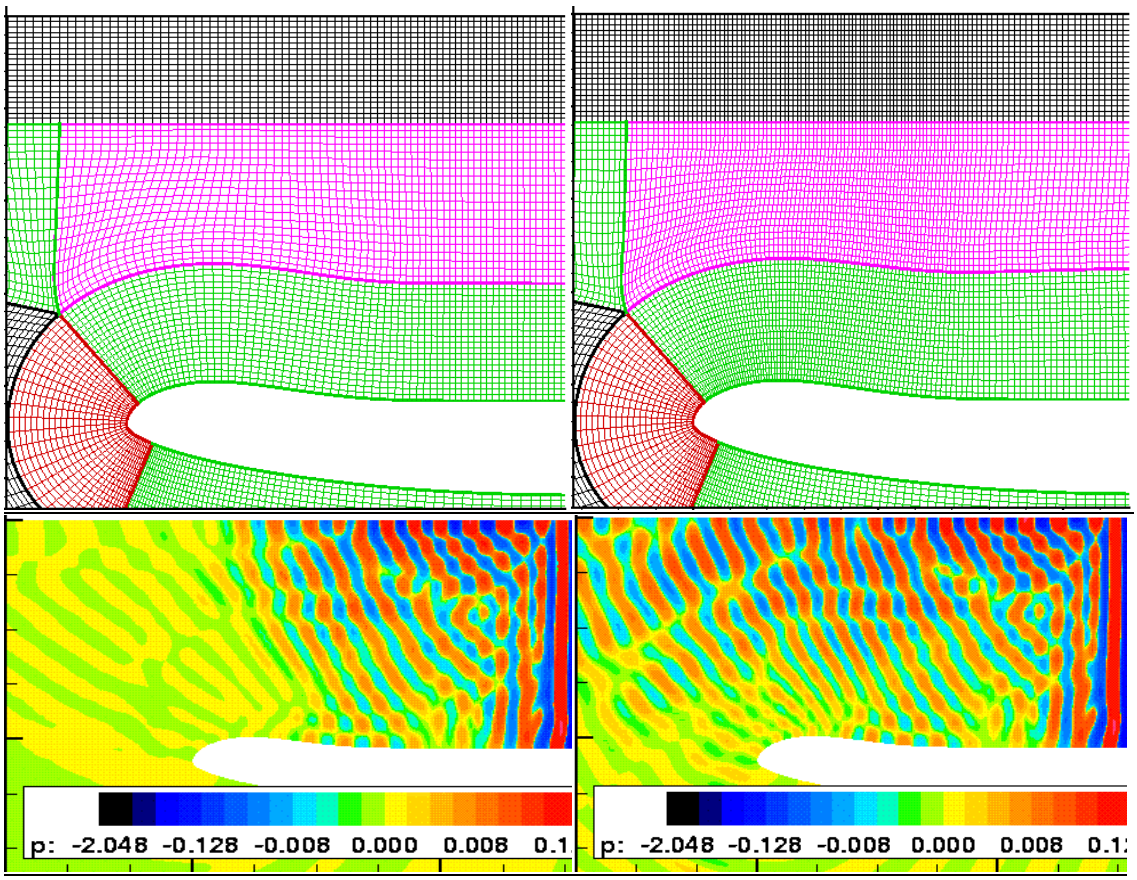

Figure 7: Influence of grid refinement with flow at Mach 0.25 and frequency 1000 Hz: original mesh (left), suitably refined mesh (right) for $^1/_2$-buried inlet, waves entering from right; detailed view

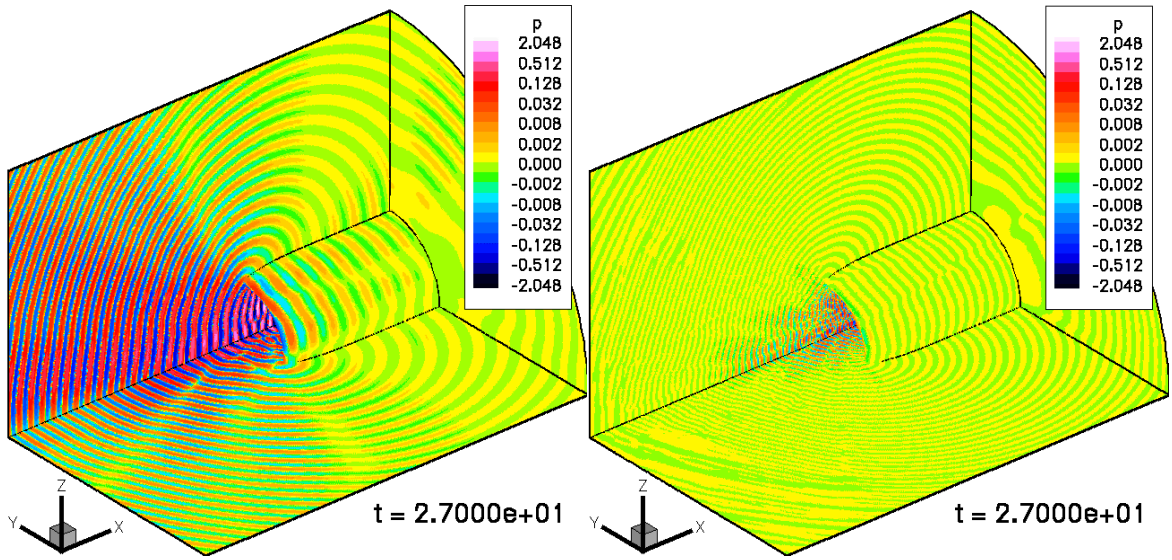

Figure 8: Influence of frequency with flow at Mach 0.25 for $^1/_2$-buried inlet:
original mesh and frequency 500 Hz (left); suitably refined mesh and frequency 1000 Hz (right)

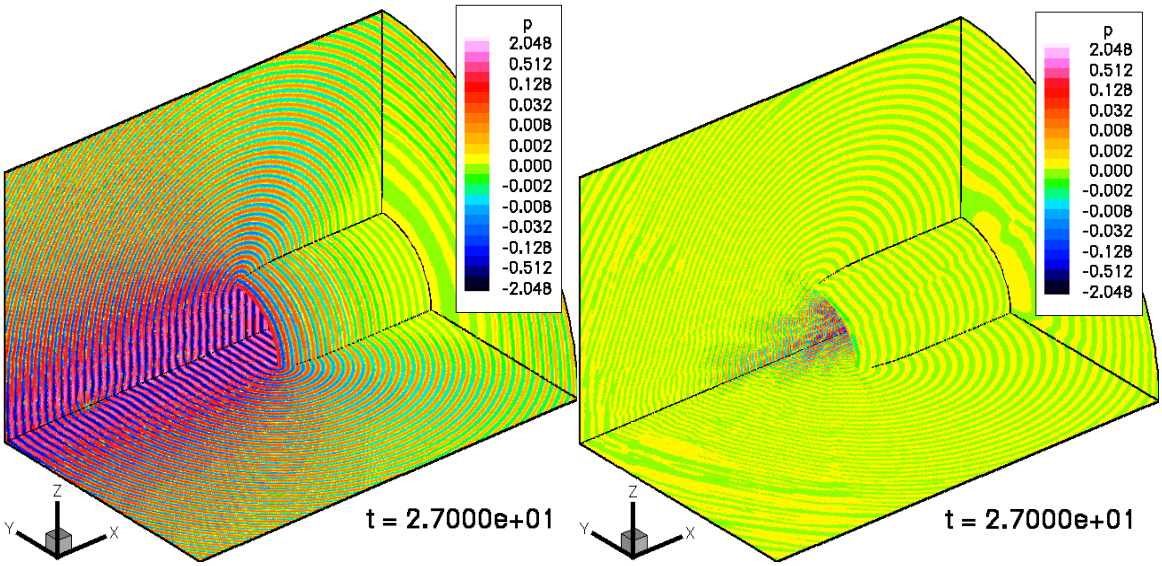

Figure 9: Influence of flow for $^1/_2$-buried inlet and frequency 1000 Hz:
without (left) and with (right) flow

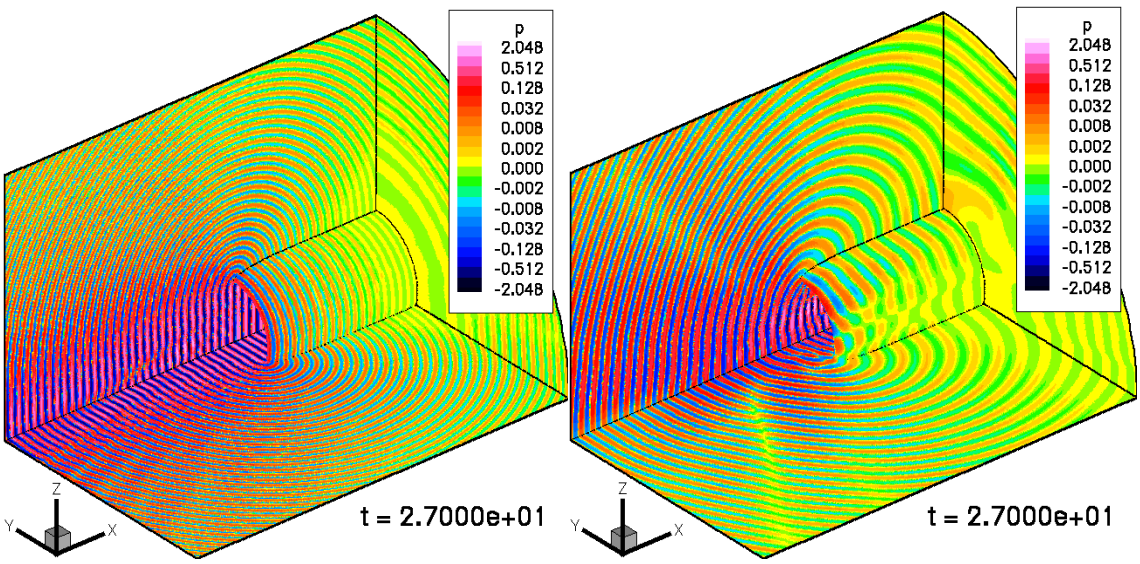

Figure 10: Influence of flow for $^1/_3$-buried inlet:
without flow and frequency 1000 Hz (left), with flow and frequency 500 Hz (right)

Comparison of burying levels

Figure 11 compares exclusively the geometric effect. Without flow the solution displays the same radiation pattern in the symmetry and ground plane for the $^1/_2$-buried geometry (left). For the $^1/_3$-buried geometry necessarily one obtains a non-axi-symmetric distribution of the sound pressure (right).

The completely axi-symmetric radiation pattern for the $^1/_2$-buried inlet (top row) and the slightly deviating solution for the $^1/_3$-buried inlet (bottom row) are displayed in several sections perpendicular to the mean flow in Figure 12. For the $^1/_2$-buried inlet the three-dimensional calculation yields the correct (exactly symmetric) structure of the pressure field as expected. This shows that the finite difference stencils and filtering techniques perform isotropically even near boundaries.

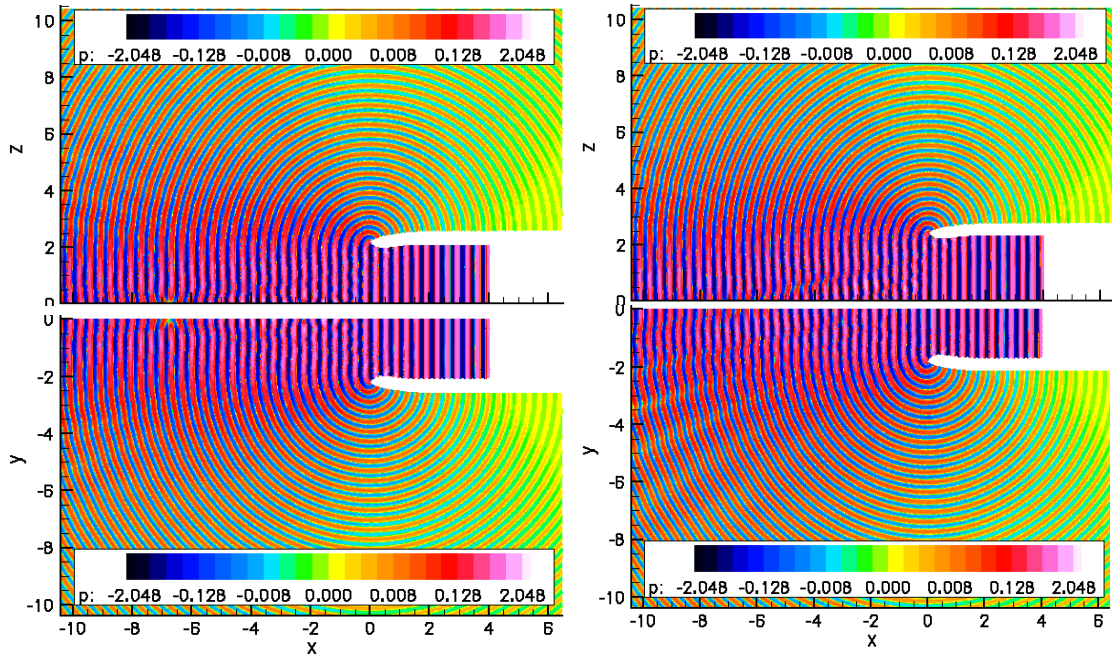

Figure 11: Influence of burying level without flow for frequency 1000 Hz:
$^1/_2$- (left) and $^1/_3$-buried inlets (right); symmetry (top) and ground plane (bottom)

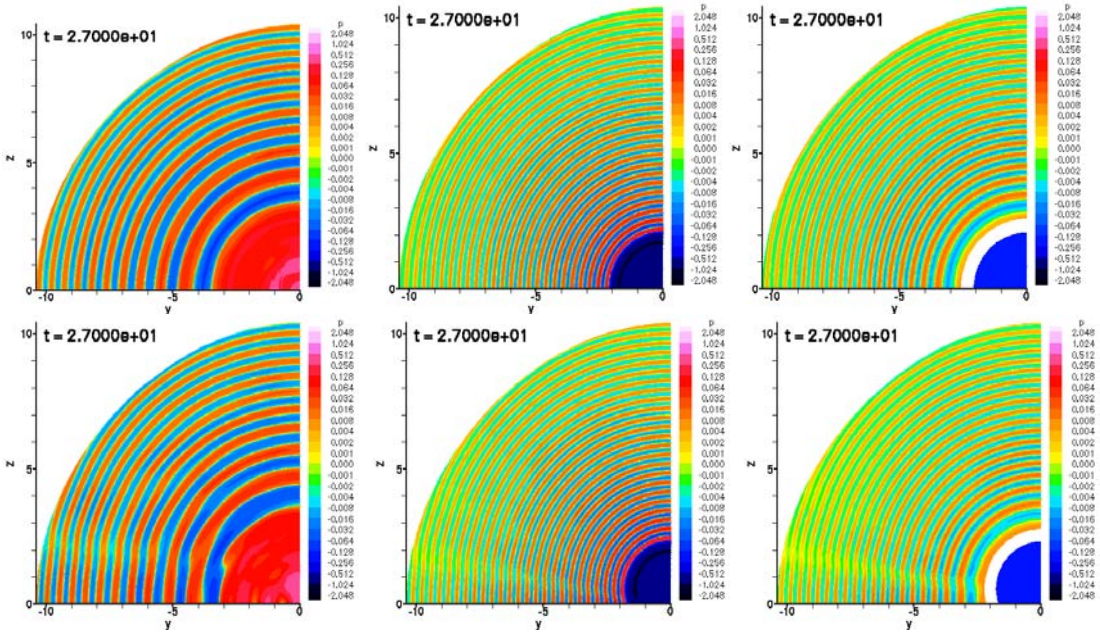

Figure 12: Axial sections up- to downstream, i.e. x = -8, x = 0, x = 2 (from left to right) without flow for $^1/_2$- (top) and $^1/_3$-buried inlet (bottom) for frequency 1000 Hz

In Figure 13 the additional mean flow effect becomes visible. In the symmetry and ground plane, a distinct lobe-structure forms with reduced radiation intensity when compared to the no-flow case. The remarkably strong influence of the flow on the radiation pattern may be appreciated on the left part of Figure 13. Since the geometry as well as the incident sound field is symmetric with respect to the fan axis, one might expect a similar radiation pattern in the symmetry plane as in the ground plane. The difference in radiation in these planes is caused by the presence of the boundary layers in the mean flow field, since due to symmetry an inviscid flow simulation would have given an axi-symmetric flow field, and necessarily a symmetric radiation pattern.

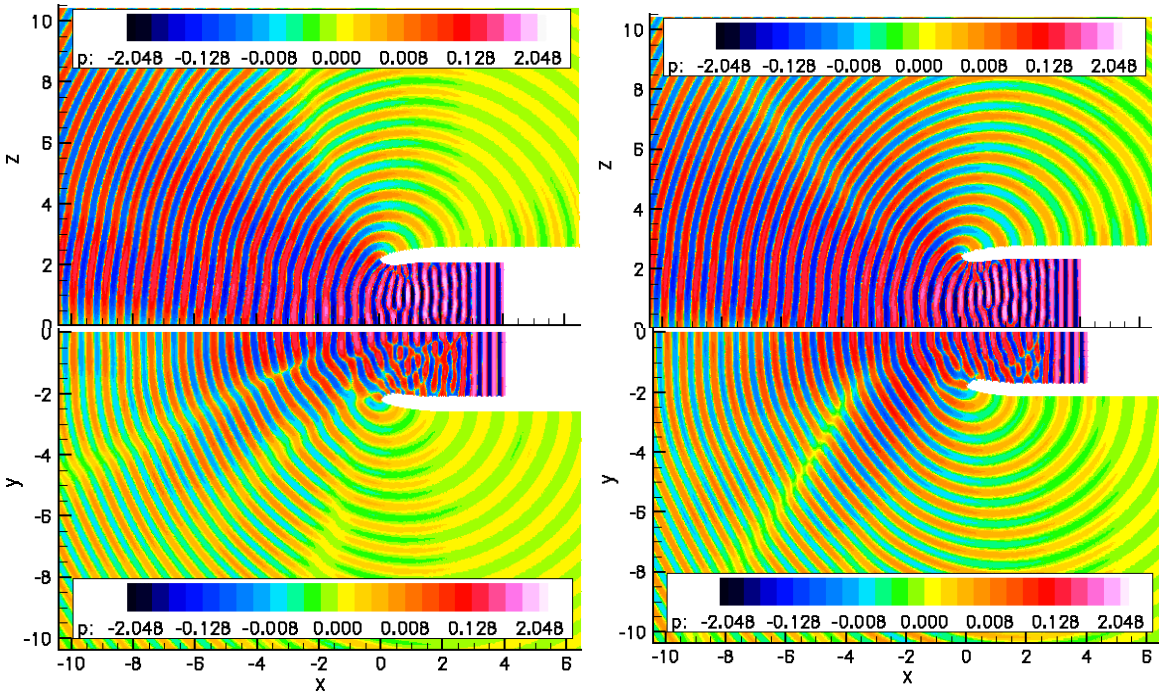

Figure 13: Influence of burying level with flow for frequency 500 Hz; $^1/_2$- (left) and $^1/_3$-buried inlet (right); symmetry (top) and ground plane (bottom)

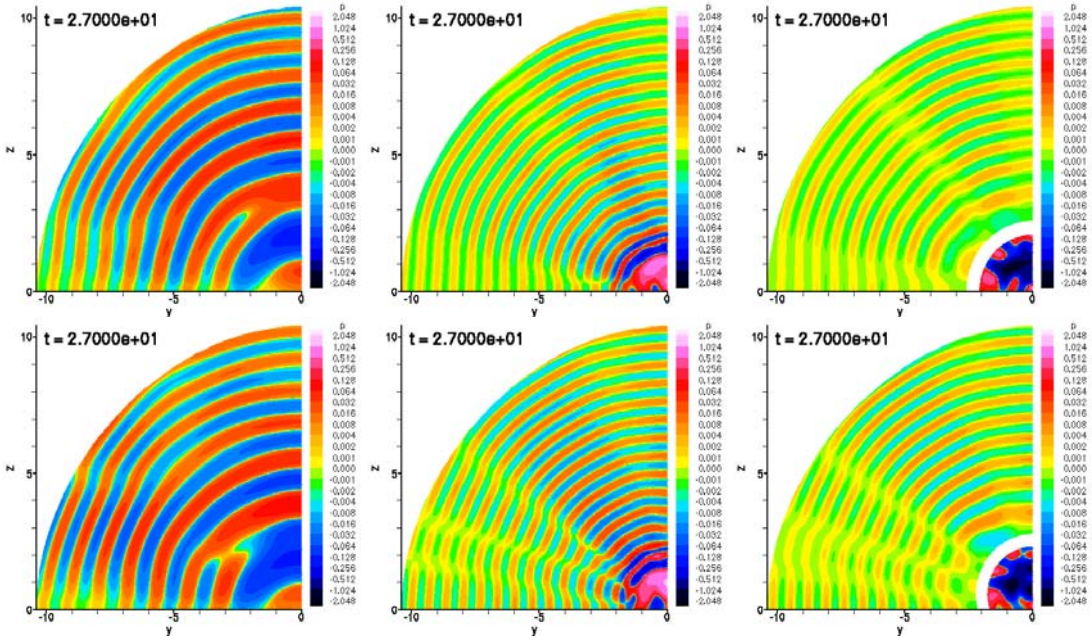

Figure 14: Axial sections up- to downstream, i.e. $x = -8$, $x = 0$, $x = 2$ (from left to right) with flow for $^1/_2$- (top) and $^1/_3$-buried inlet (bottom) for frequency 500 Hz

Figure 14 depicts the structure of the radiation pattern for different sections perpendicular to the mean flow, for the $^1/_2$- (top row) and the $^1/_3$-buried inlets (bottom row). Again, the presence of the viscous mean flow introduces a remarkable lateral direction dependence even for the $^1/_2$-buried (symmetric) geometry. The effect on the lateral directivity is shown in the left part of Figure 15.
The main effect of burying the intake $^1/_3$ of the diameter instead of $^1/_2$ of the diameter is seen in an increased overall three-dimensionality of the radiation directivity. The overall noise output is changed insignificantly, provided the source is identical.

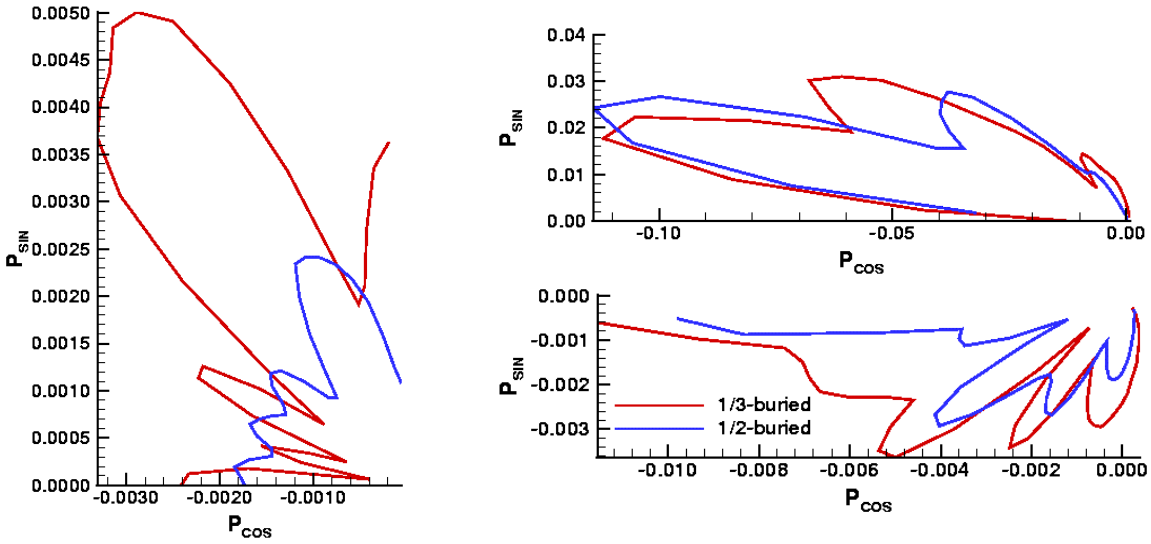

Figure 15: Directivity with flow for $^1/_2$- and $^1/_3$-buried inlet in lateral (left), symmetry (top right) and ground plane (bottom right) for frequency 500 Hz

Conclusions

The radiation characteristics of simplified engine fan tones from two generic semi-buried air intakes have been predicted. The objective of the investigation was to show the sound diffraction and shielding effect of the different intake configurations for take-off conditions.
A RANS mean flow calculated with the DLR Tau code was linearly interpolated from the unstructured CFD mesh onto the structured CAA grid. The CAA grid must be defined carefully because an only locally too poor grid resolution may result in a completely non-physical solution. The computations lead to the following conclusions:

- Without flow, the $^1/_3$-buried inlet causes a non-axi-symmetric lateral directivity, contrary to the $^1/_2$-buried inlet for which it is axi-symmetric.
- The actual viscous mean flow plays an important role: especially (even poorly resolved) boundary layers cause a considerable modification of the directivity for the two inlet shapes.
- With mean flow, the most significant differences between the $^1/_2$- and $^1/_3$-buried inlet are observed on the lateral directivity; on a general picture, the burying level has a small influence only.
- No excitation of flow instabilities, nor self sustained flow oscillations (resonances) were observed in any considered case.
- The boundary layer on the surface into which the intake is buried causes a 'zone of silence' effect upstream, which may be beneficial for respective aircraft concepts, as far as noise is concerned.

The results underline the need for using a perturbation approach of LEE type to describe the physics of the sound radiation from an buried intake properly.

Acknowledgements

The authors would like to thank Airbus S. A. S. for financially supporting this work within the SeBu project.

References

Y. Kallinderis, A. Khawaja and H. McMorris, *Adaptive Hybrid Prismatic-Tetrahedral Grids for Viscous Flows*, Proceedings of the Surface Modeling, Grid Generation and Related Issues in Computational Fluid Dynamics Workshop, NASA Conference Publication 3291, p. 311, NASA Lewis Research Center, Cleveland, OH, May 1995; CentaurSoft, http://www.centaursoft.com

N. Kroll, J. K. Fassbender (Eds.), *MEGAFLOW – Numerical Flow Simulation for Aircraft Design*, Notes on Numerical Fluid Mechanics and Multidisciplinary Design (NNFM), 89, 2005, Springer

M. Lummer, H. A. Grogger and J. W. Delfs; *Using RANS Mean Flow Fields in Numerical Aeroacoustics Simulations (CAA)*, RTO/AVT Symposium on Aging Mechanisms and Control, Part A - Development in Computational Aero- and Hydro-Acoustics, Manchester, UK, 8-11 October 2001

J. S. Shang; *High-Order Compact-Difference Schemes for Time-Dependent Maxwell Equations*, Journal of Computational Physics, 153, pp. 312-333, 1999

C. K. W. Tam and J. C. Webb; *Dispersion-Relation-Preserving Finite Difference Schemes for Computational Acoustics*, Journal of Computational Physics, 107, pp. 262-281, 1992

C. K. W. Tam, J. C. Webb and Z. Dong; *A study of the short wave components in computational Acoustics*, Journal of Computational Acoustics, 1, pp. 1-30, 1993

C. K. W. Tam and Z. Dong; *Wall boundary conditions for high-order finite-difference schemes in computational aeroacoustics*, Theoretical Computational Fluid Dynamics, 6, pp. 303-322, 1994

Oleg V. Vasilyev, Thomas S. Lund and Parviz Moin; *A General Class of Commutative Filters for LES in Complex Geometries*, Journal of Computational Physics, 146, pp. 82-104, 1998